Modeling Surfactant Adsorption on Hydrophobic Surfaces

Steve O. Nielsen,* Goundla Srinivas, Carlos F. Lopez, and Michael L. Klein

Center for Molecular Modeling and Department of Chemistry, University of Pennsylvania, Philadelphia, Pennsylvania 19104-6323, USA

(Received 22 October 2004; published 8 June 2005)

Surfactant adsorption on hydrophobic surfaces is of current interest in attempts to solubilize single-wall carbon nanotubes and to render quantum dots biocompatible. A coarse grained method is presented for incorporating a hydrophobic surface into existing liquid force fields by appealing to statistical mechanics and probability theory. The dimensionality problem which arises is overcome with an approximate treatment and the entire procedure is applied to aqueous *n*-alkyl poly(ethylene oxide) adsorbing onto a graphite surface. The simulations are in excellent agreement with atomic force microscopy data. The mechanism of micelle adsorption onto a partially coated surface is reported for the first time and has implications for the construction of nanotemplates.

DOI: 10.1103/PhysRevLett.94.228301 PACS numbers: 82.70.Uv, 61.20.Ja, 68.08.-p, 68.43.Jk

The tendency of surfactants to self-assemble on or around a hydrophobic surface in an aqueous environment is being exploited to great effect in both materials and biological settings. Surfactant solubilization of single-wall carbon nanotubes (SWNTs) in water is recognized as one of the most promising routes to manipulate nanotubes into useful constructs [1,2]. However, the SWNT solubilization and stabilization characteristics vary considerably between chemically and structurally similar surfactants, and even the adsorbate morphology is the subject of debate [1–3]. In a biological context, surfactants have been successfully used to solubilize hydrophobic quantum dots, prevent their nonspecific adsorption and aggregation, render them biocompatible, and stabilize them for long periods of time [4]. A molecular level understanding of these self-assembly processes and the morphology of the resulting surfactant-coated substrate is lacking because the length and time scales of relevance largely fall outside of the scope of both experimental techniques and fully atomistic computer simulations. In this Letter, a general method is presented for incorporating a hydrophobic surface into coarse grained liquid force fields, which are designed to access precisely the relevant length and time scales, and which have been shown to accurately model polymer and other macromolecular systems [5–9]. The presentation begins by replacing the explicit hydrophobic surface with an implicit potential. The coarse graining is then performed by using probability theory to combine atomistic interactions into effective center of mass interactions, and as a final step the surface is restored to an explicit representation.

The simplest implicit description is constructed, from the potential $u(r)$ between an individual atom in the surface and an atom in the liquid phase, by approximating the surface as a continuum with number density ρ that occupies the semi-infinite region $z \leq 0$. An atom belonging to the liquid phase at a height $z > 0$ interacts with the surface via [10]

$$\begin{aligned} U(z) &= \int_z^\infty dr \int_0^{2\pi} d\theta \int_{\pi-\cos^{-1}(z/r)}^{\pi} d\phi r^2 \sin\phi \rho u(r) \\ &= 2\pi\rho \int_z^\infty r u(r)[r - z] dr \\ &= \frac{4}{45} \frac{\pi\rho\epsilon\sigma^{12}}{z^9} - \frac{2}{3} \frac{\pi\rho\epsilon\sigma^6}{z^3} \end{aligned} \tag{1}$$

where for the last expression the Lennard-Jones potential $u(r) = 4\epsilon[(\sigma/r)^{12} - (\sigma/r)^6]$ has been used. This description assumes a flat interface, but this constraint is removed later when the explicit representation is reestablished. Next, the system is coarse grained by replacing a group of atoms in the liquid phase by their center of mass (c.m.) and calculating the effective interaction between the c.m. and the surface. To achieve this, the interactions are described, not in terms of potential energies, but in terms of probability distributions. The probability and the potential are related by $\mathcal{P} = e^{-\beta U}$ where β is the inverse of Boltzmann's constant times the temperature. Note that the normalization convention for $\mathcal{P}$ is, in analogy to the pair correlation function, that the probability reaches unity in the limit of infinite separation. For the simplest case of two identical noninteracting particles, the joint probability of finding particle 1 at height z_1 and particle 2 at height z_2 above the surface is given by

$$\mathcal{P}(z_1, z_2) = e^{-\beta U(z_1)} e^{-\beta U(z_2)}, \tag{2}$$

since the individual surface-particle potentials are additive. The probability of the center of mass being at height z is given by

$$\mathcal{P}(z) = (2z)^{-1} \int_0^{2z} e^{-\beta U(z_1)} e^{-\beta U(2z - z_1)} dz_1. \tag{3}$$

The straightforward manner in which the joint probability distribution is converted to the c.m. marginal distribution is precisely the reason for formulating the problem in this manner.

For two identical interacting particles the joint probability distribution becomes

$$\mathcal{P}(z_1, z_2) = e^{-\beta U(z_1)} e^{-\beta U(z_2)} \mathcal{P}_I(z_1, z_2). \quad (4)$$

The joint distribution is the product of three terms since the corresponding potential is composed of the sum of two particle-surface terms and an interaction term $\mathcal{P}_I$ between the particles which does *not* involve the surface. The independence of the interaction term from the solid surface stems from the widely accepted use of effective two-body forces in condensed matter atomistic force fields.

Returning to Eq. (4), the probability of the center of mass being at height z may be formulated as

$$\mathcal{P}(z) = \frac{\int_0^{2z} e^{-\beta U(z_1)} e^{-\beta U(2z-z_1)} \mathcal{P}_I(2z_1 - 2z) dz_1}{\int_0^{2z} \mathcal{P}_I(2z_1 - 2z) dz_1} \quad (5)$$

where the normalization constant is the numerator evaluated at $U \equiv 0$, namely, with no surface. This probability distribution is shown in Fig. 1(a) and the corresponding potential is shown in Fig. 1(c). The calculation of the distribution at the marked point in Fig. 1(a) is shown in detail in Fig. 1(b) by plotting the three underlying probability distributions constituting Eq. (4). In Eqs. (3) and (5) the integration over the z coordinate of the first particle is performed by eliminating the z coordinate of the second particle using the center of mass constraint $z_2 = 2z - z_1$. The interaction term $\mathcal{P}_I(z_1, z_2)$ is equal to $\mathcal{P}_I(z_1 - z_2) = \mathcal{P}_I(2z_1 - 2z)$ up to a normalization constant which cancels in the numerator and denominator of Eq. (5). As a result of these considerations the two individual particle-surface terms are reflections of one another in the line $z_1 = z$ [see Fig. 1(b)]. In Fig. 1(b) the interaction term, which constrains the two particles to remain close together since it arises from a chemical bond, selects the region of maximal overlap between the two surface-particle interactions. Without this restriction, the maximal overlap region is diluted by the overlap of the full particle-surface curves. This is precisely the difference between expressions (3) and (5) and results in the enhanced probability and correspondingly deeper well depth for the bonded as opposed to the noninteracting particles shown in Fig. 1(c). It should also be noted that the equilibrium distance from the surface shifts to larger values as the number of particles included in the coarse grained site increases.

The generalization of Eq. (5) to many particles of unequal masses and unequal interactions with the surface is straightforward. However, some difficulties arise in evaluating the resulting terms. For the case of two particles attached by a harmonic bond with potential energy U_{harm}, the interaction distribution $\mathcal{P}_I$ can be obtained directly from $\mathcal{P}_I = e^{-\beta U_{\text{harm}}}$. In general, however, a fully atomistic simulation is needed to capture subtle conformational effects. For example, poly(ethylene oxide) adopts an all- *cis* conformation in vacuum, but an all-*trans* conformation is preferred in water; an aqueous simulation must be performed to properly obtain the $\mathcal{P}_I$ distributions involving bending and torsional potentials. Furthermore, since the surface is absent in this simulation, it is required by symmetry that $\mathcal{P}_I$ be unchanged under coordinate axis rotation. In practice, the simulation box is rotated as the coordinates are sampled to enforce symmetry.

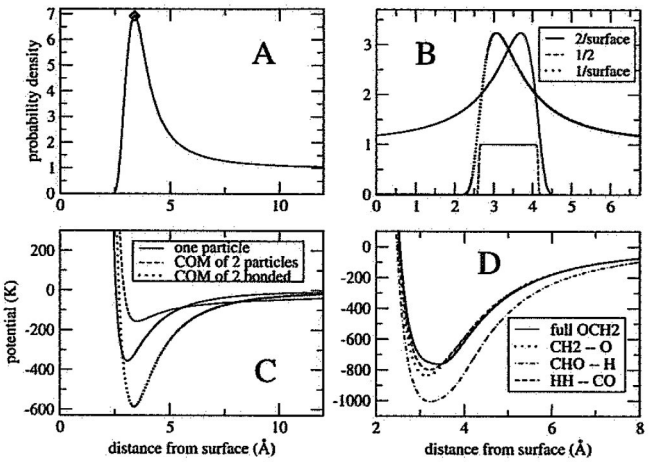

FIG. 1. (a) The probability distribution for the center of mass of two bonded particles interacting with the surface [see Eq. (5)]. The distribution is normalized to reach unity in the limit of infinite separation. The single particle—graphite parameters [see Eq. (1)] are $\rho = 0.113$ Å^{-3} (the graphite site is an sp^2 hybridized carbon atom) and $\epsilon = 31.51$ K, $\sigma = 3.566$ Å, which is the CTL2 carbon atom from CHARMM [22]. The CTL2-CTL2 bond is harmonic with $k = 223\,934$ K Å^{-2} and $r_{\text{eq}} = 1.53$ Å. (b) The probability distribution for a fixed center of mass value $z = 3.38$ Å, which corresponds to the circle in panel (a), of two bonded particles interacting with the surface from Eq. (5). Shown is the integrand in the numerator broken down into its three constituent terms, where the interaction term is normalized to have unit height for clarity since the denominator in Eq. (5) corrects for this arbitrary choice. The bond constrains the two particles to reside close to the center of mass and enhances the well depth over the noninteracting case. (c) Comparison of the potential experienced by one particle, and the potential experienced by the center of mass of two noninteracting particles, and two bonded particles. Parameters as in panel (a). (d) The effective potential experienced by the center of mass of an -O-CH_2- piece of poly(ethylene oxide) due to a graphite surface at $z = 0$, and three approximations based on integrals of reduced dimensionality (see the text for details).

Another difficulty is the high dimensionality of both the integration and the interaction probability $\mathcal{P}_I$; in the coarse grain (CG) approach it is common to include three or more heavy atoms and their accompanying hydrogen atoms into a single site [7–9]. This problem can be tackled with an appropriate Monte Carlo integration method. Instead, we will apply an iterative procedure to reduce the calculation to a series of low-dimensional expressions. Each heavy atom is combined with its accompanying hydrogen atoms into a united atom site [11]. The united atom sites are combined in one or several steps to obtain the final CG

representation. This procedure is illustrated on a -O-CH_2- piece of poly(ethylene oxide) interacting with a graphite surface. The full three dimensional (four atom) expression is evaluated and presented in Fig. 1(d), along with three approximations obtained using the following schemes: (i) the CH_2 unit is coarse grained, and then this unit is combined with the oxygen atom; (ii) a CHO unit is coarse grained, and then combined with the remaining hydrogen atom; (iii) the HH and CO di-atoms are coarse grained separately, and then combined. Approximations (i) and (iii) are reasonable, while (ii) is in significant error. Scheme (i) is the natural reduction; the hydrogen atoms are combined with their associated heavy atom into a united atom site. Scheme (iii) is reasonable based on symmetry, while Scheme (ii) is not natural and is not reasonable from either symmetry or chemical grounds. In practice we use Scheme (i)—namely, the united atom approach. In this manner the error introduced by the dimensionality approximations is minimized.

To apply the foregoing considerations in a more realistic context, we treat the case of aqueous *n*-alkyl poly(ethylene oxide) (CnEm) adsorbing onto a graphite surface. The surface potentials are available on our web site [12,13].

The self-assembly structures of nonionic surfactants at graphite-liquid interfaces have been extensively characterized by atomic force microscope (AFM) and other experimental methods. In particular, C9E3, which is geometrically capable of only forming bilayers as a bulk lyotropic phase, forms monolayers perpendicular to the graphite surface [14]. C12E5, which is capable of forming cylindrical micelles in solution, is found to form hemicylinders at the graphite-liquid interface [15].

In the present CG model, the nonionic surfactant CnEm is represented by $n/3$ and m CG sites, respectively, giving a mapping of three CH_2 groups per hydrophobic site and one ethylene oxide monomer per hydrophilic site. This level of coarse graining preserves the overall shape of the surfactants, which is crucial in determining their self-assembled morphology. In previous studies we developed the CG parameters for poly(ethylene oxide)—poly(ethyl ethylene) diblock copolymers and alkane chains; these parameters have been used here for the liquid-liquid interactions [9,16,17]. The surfactants have harmonic bonds and bends obtained from fully atomistic simulation data and nonbonded interactions derived primarily from experimental bulk density, surface tension, and liquid-liquid interfacial tension data. Diffusion coefficients were calculated from mean square displacement curves for various concentrations of binary mixtures of C12E5 and water (data not shown) and the results obtained are in close agreement with experiment [18].

Snapshots from simulations of C12E5 adsorption onto a graphite surface are presented in Fig. 2. The surfactants, initially dispersed randomly throughout the aqueous phase, either begin to coat the graphite surface or start self-assembling into spherical micelles in the bulk water away from the surface. Despite the occasional interactions, these aggregates never fuse into a single micelle, demonstrating that they are well saturated. In the process of random motion the micelles diffuse toward either of the graphite surfaces. A remarkable adsorption mechanism is observed once the micelle reaches the vicinity of the graphite surface. The micellar surfactant head groups near the surface interact with those of the surfactants already adsorbed on graphite. At this point, we find that the micelle starts ''feeding'' the graphite surface [Figs. 2(c) and 2(d)].

The two sets of head groups pull away to allow direct contact between the hydrophobic tails of the micellar surfactants and those of the flat monolayer. The hydrophobic micelle tails then drain very quickly onto the graphite surface, with concomitant rearrangement of the head groups. In this manner the entire micelle is adsorbed onto the surface.

Once the adsorption process is completed, the reorganization starts. The self-organization on a graphite surface in this case results in the formation of hemicylinders as shown in Fig. 2(f). This is the first study to observe hemicylinder formation on a solid substrate in simulations. The lateral spacing between hemicylinders is calculated as 5.0 ± 0.4 nm, which is in very good agreement with the experimental data of 4.7 ± 0.3 nm [19].

Simulations with C9E3 surfactant also show the aggregate feeding mechanism, but with a different final state. As the extent of feeding increases, the thickness of the partially coated monolayer also increases, indicating that the surfactants start changing their orientation from near parallel to perpendicular to the surface. The C9E3 adsorption leads to an aggregate with the shape of a near perfect monolayer on the graphite surface (not shown), which

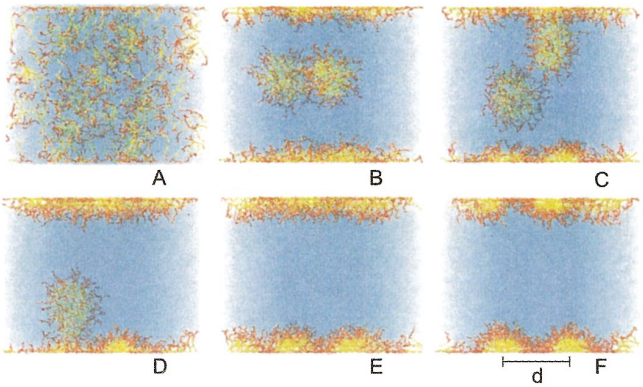

FIG. 2 (color). Snapshots of C12E5 surfactant adsorption onto a graphite surface as observed in simulations, at times of 0, 0.64, 3.30, 3.75, 4.30, and 6.00 ns, respectively. There are solid-liquid interfaces at the top and bottom of the simulation cell which are separated by 12 nm through the water and by 10 nm through vacuum (not shown); three dimensional periodic boundary conditions are employed.

continues to reorganize itself until it forms a monolayer coating the surface, in agreement with experiment. However, the complete adsorption of micelles onto the surface indicates that the surfactant concentration might not be saturated.

In addition to surfactant adsorption, alkane mixtures display a wide range of behavior in the presence of a graphite surface. For example, the shorter chain species in binary mixtures of n-alkanes can preferentially adsorb at the surface at a high enough mole fraction [20]. We have reproduced this trend with our simulations [21].

We now turn to recovering an explicit representation of the surface. This will allow for a greater range of surface geometries to be considered, from more detailed studies of flat surfaces, to studies with cylindrical nanotubes and spherical quantum dots, and to studies with more complicated geometries such as modeling an AFM tip. The key is to realize that Eq. (1), which we restate here as $U(z) = 2\pi\rho \int_z^\infty ru(r)[r - z]dr$, and which was used to move from a known explicit representation to an implicit representation, can be reversed. The surface potential experienced by a CG unit, which was derived according to the methods presented above, is used to recover an explicit potential by taking two derivatives to yield $u(\xi) = U''(\xi)/(2\pi\rho\xi)$. Here ρ represents the level of coarse graining of the surface and is a free parameter; however, it must match the explicit representation used in the simulation.

The methods outlined in this paper are aimed at facilitating nanometer scale studies of the structure and dynamics of hydrophobic surfaces interacting with aqueous surfactant solution. The computational savings are about 4 orders of magnitude compared to a fully atomistic calculation; this results from having fewer pairwise interactions to evaluate and from having softer potentials, which allow for a larger integration time step and which lead to enhanced diffusion [9]. In particular, these methods should aid in developing a detailed physical understanding of the relative ability of different surfactants to solubilize carbon nanotubes. Although not the main focus of this Letter, the simulation studies we report showing micelle absorption onto a graphite surface suggest a novel method for depositing quantum dots on a substrate. Libchaber *et al.* [4] have shown how to encapsulate quantum dots in aqueous surfactant micelles which are not appreciably perturbed in their geometry or size. It would be interesting to study such micelle-encapsulated quantum dots in the presence of a solid substrate to see what nanotemplating and deposition patterns result.

*Email address: snielsen@cmm.upenn.edu
Electronic address: http://www.cmm.upenn.edu/~snielsen

[1] M. J. O'Connell, S. M. Bachilo, C. B. Huffman, V. C. Moore, M. S. Strano, E. H. Haroz, K. L. Rialon, P. J. Boul, W. H. Noon, C. Kittrell, J. Ma, R. H. Huage, B. R. Weisman, and R. E. Smalley, Science **297**, 593 (2002).
[2] M. F. Islam, E. Rojas, D. M. Bergey, A. T. Johnson, and A. G. Yodh, Nano Lett. **3**, 269 (2003).
[3] K. Yurekli, C. A. Mitchell, and R. Krishnamoorti, J. Am. Chem. Soc. **126**, 9902 (2004).
[4] B. Dubertret, P. Skourides, D. J. Norris, V. Noireaux, A. H. Brivanlou, and A. Libchaber, Science **298**, 1759 (2002).
[5] B. Smit, P. A. J. Hilbers, K. Esselink, L. A. M. Rupert, N. M. van Os, and A. G. Schlijper, Nature (London) **348**, 624 (1990).
[6] R. Goetz, G. Gompper, and R. Lipowsky, Phys. Rev. Lett. **82**, 221 (1999).
[7] H. Fukunaga, J. Takimoto, and M. Doi, J. Chem. Phys. **116**, 8183 (2002).
[8] F. Müller-Plathe, Chem. Phys. Chem. **3**, 754 (2002).
[9] S. O. Nielsen, C. F. Lopez, G. Srinivas, and M. L. Klein, J. Phys. Condens. Matter **16**, R481 (2004).
[10] T. L. Hill, *An Introduction to Statistical Thermodynamics* (Dover, New York, 1986).
[11] J. D. McCoy and J. G. Curro, Macromolecules **31**, 9362 (1998).
[12] Available at www.cmm.upenn.edu/~snielsen/
[13] We determine the water or graphite parameters by demanding that the CG water form a droplet on the CG graphite surface with a contact angle of $\theta_\infty = 86°$, using the methodology of Werder [23] (see Fig. 1 of Werder [23]; we use a droplet of 22000 CG water particles, which corresponds to 66000 real water molecules).
[14] W. A. Ducker and L. M. Grant, J. Phys. Chem. B **100**, 11507 (1996).
[15] H. N. Patrick, G. G. Warr, S. Manne, and I. A. Aksay, Langmuir **13**, 4349 (1997).
[16] G. Srinivas, J. C. Shelley, S. O. Nielsen, D. E. Discher, and M. L. Klein, J. Phys. Chem. B **108**, 8153 (2004).
[17] S. O. Nielsen, C. F. Lopez, G. Srinivas, and M. L. Klein, J. Chem. Phys. **119**, 7043 (2003).
[18] E. Feitosa, W. Brown, M. Vasilescu, and M. Swanson-Vethamuthu, Macromolecules **29**, 6837 (1996).
[19] S. Manne and H. E. Gaub, Science **270**, 1480 (1995).
[20] M. A. Castro, S. M. Clarke, A. Inaba, R. K. Thomas, and T. Arnold, J. Phys. Chem. B **105**, 8577 (2001).
[21] See EPAPS Document No. E-PRLTAO-94-010525 for supplementary information showing some additional results. A direct link to this document may be found in the online article's HTML reference section. This document may also be reached via the EPAPS homepage (http://www.aip.org/pubservs/epaps.html) or from ftp.aip.org in the directory /epaps/. See the EPAPS homepage for more information.
[22] B. R. Brooks, R. E. Bruccoleri, B. D. Olafson, D. J. States, S. Swaminathan, and M. Karplus, J. Comput. Chem. **4**, 187 (1983).
[23] T. Werder, J. H. Walther, R. L. Jaffe, T. Halicioglu, and P. Koumoutsakos, J. Phys. Chem. B **107**, 1345 (2003).